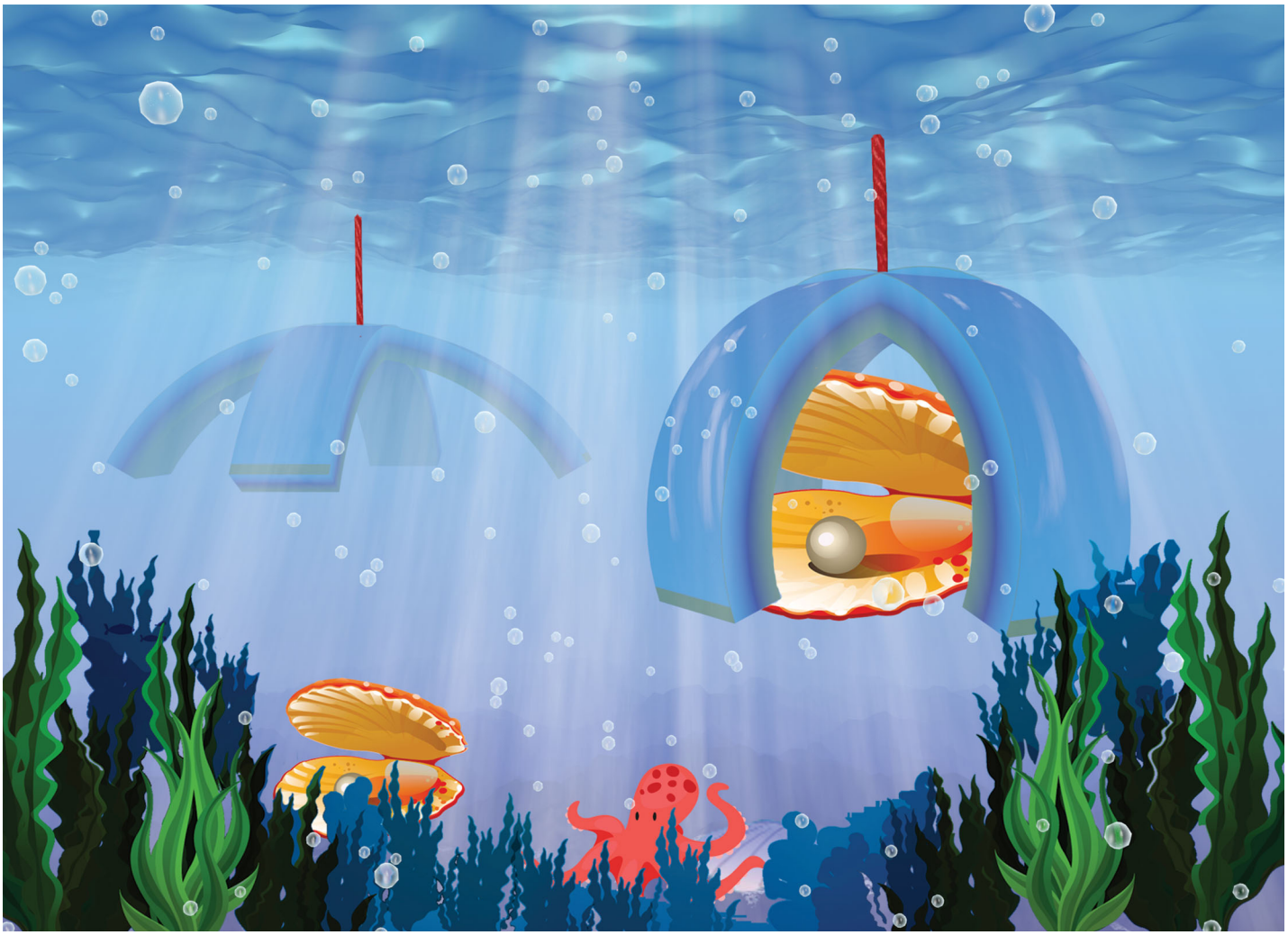

Showcasing research from Zhejiang Sci-Tech University, Zhejiang University of Technology and Xi'an Jiaotong University, P. R. China.

Gradient porous PNIPAM-based hydrogel actuators with rapid response and flexibly controllable deformation

Temperature-responsive, gradient structured PNIPAM-based intelligent hydrogel with bidirectional bending properties can realize flexibly controllable deformation and activity which will have applications as programmable and versatile hydrogel-based smart actuators and soft robots.

As featured in:

See Aiping Liu, Fangmin Ye *et al.*, *J. Mater. Chem. C*, 2020, **8**, 12092.

ROYAL SOCIETY OF CHEMISTRY

rsc.li/materials-c

Registered charity number: 207890

Journal of Materials Chemistry C

ROYAL SOCIETY OF CHEMISTRY

PAPER

View Article Online
View Journal | View Issue

Cite this: J. Mater. Chem. C, 2020, 8, 12092

Gradient porous PNIPAM-based hydrogel actuators with rapid response and flexibly controllable deformation†

Jian Liu,‡[a] Weizhong Xu,‡[a] Zhongwen Kuang,[a] Pengli Dong,[a] Youxing Yao,[a] Huaping Wu,[b] Aiping Liu *[ac] and Fangmin Ye*[a]

Received 9th January 2020,
Accepted 1st June 2020

DOI: 10.1039/d0tc00139b

rsc.li/materials-c

Smart hydrogels play a vital role in fundamental research and industrial applications in the fields of biosensors, flexible devices and intelligent human–machine technologies; however, developing a simple, low-cost and large-scale method to obtain hydrogel actuators with rapid response and robust and steadily controllable motion remains a big challenge. In this work, a temperature-responsive, gradient structured hydrogel with quick bending and adjustable actuation was fabricated by the copolymerization of the *N*-isopropylacrylamide (NIPAM) monomer with dispersed montmorillonite (MMT) *via* a facile precipitation method. The introduction of MMT with good thermal conductivity made the volume phase transition of the PNIPAM-based hydrogel occur earlier, and the deformation degree and bending direction could be adjusted by changing the MMT content. The representative composite hydrogel with 0.2 g MMT in the precursor presented bidirectional bending characteristics with a bending amplitude of about 289° and an average bending speed of about 36.0° s^{-1}, while the composite hydrogel with 0.3 g MMT in the precursor only possessed a unidirectional bending ability with a bending amplitude of about −259° and a bending velocity of about −28.8° s^{-1} due to the great difference in the shrinking capacity between the top and bottom sides of the composite hydrogel. In addition, flexibly controllable deformation was specially realized by a well-designed patterned hydrogel with a local component and a thickness difference. Our work provides a practical method for the ingenious design of a hydrogel for further development of programmable and versatile hydrogel-based smart actuators and soft robots.

1. Introduction

Intelligent actuators, showing potential applications in soft robots,[1–3] microfluidic valves,[4] biosensors,[5–8] and smart drivers,[9,10] have been given extensive attention. Among them, hydrogel-based actuators, which mainly utilize the great changes in volume and/or shape induced by external stimuli such as temperature,[11–14] humidity,[15,16] pH or ion concentration difference,[17–19] and electric[20–23] or magnetic field,[24–26] have become alternatives for intelligent actuators. The origin of the bending/unbending of a smart hydrogel under stimuli[27] is mainly due to the unbalance of the internal stress of the hydrogel which is induced by different magnitudes of expansion/shrinking in different directions.[28] Therefore, to design the anisotropic structure of hydrogel actuators is crucial for steering their actuation behaviors.

To realize the anisotropic structure of a hydrogel, one of the traditional strategies used is to create a bilayer structure[29–32] with a passive polymer hydrogel and an active one. However, this bilayer tends to delaminate along the weak interface after repetitive actuation.[33] Another effective means is to construct a gradient structured hydrogel, which enables us to controllably adjust its driving behavior.[34] For example, LAPONITE® was used as a cross-linking agent and an initiator agent of gradient distribution during the course of the hydrogel polymerization to obtain a gradient structured hydrogel.[35] However, such hydrophilic nanoparticles as LAPONITE® could generate poor temperature-response characteristics of the hydrogel.[36] Furthermore, the gradient cross-linked structure of the smart hydrogel with temperature response could also be produced by controlling the preparation conditions, such as UV irradiation.

[a] Center for Optoelectronics Materials and Devices, Key Laboratory of Optical Field Manipulation of Zhejiang Province, Zhejiang Sci-Tech University, Hangzhou 310018, P. R. China. E-mail: liuaiping1979@gmail.com, fmye2013@sinano.ac.cn
[b] Key Laboratory of Special Purpose Equipment and Advanced Processing Technology, Ministry of Education and Zhejiang Province, College of Mechanical Engineering, Zhejiang University of Technology, Hangzhou 310023, China
[c] State Key Laboratory for Strength and Vibration of Mechanical Structures, School of Aerospace Engineering, Xi'an Jiaotong University, Xi'an 710049, P. R. China

† Electronic supplementary information (ESI) available. See DOI: 10.1039/d0tc00139b

‡ J. Liu and W. Xu contributed equally to this work.

Fan *et al.*[37] reported that a hydrogel precursor with a dispersion of graphene oxide nanosheets could be developed under UV irradiation and a gradient cross-linking structure was finally obtained by gradually weakening the UV light with incident depth. In addition, fabricating heterogeneous structures of hydrogel actuators[38] by including orientated magnetic particles,[39] changing local gel thickness,[33,40] or introducing porous structures[41] could also successfully adjust the bending speed and deformation degree of hydrogel actuators. However, the construction of porous heterogeneous structures might deteriorate the mechanical properties of the hydrogel. Therefore, how to maintain the balance between the significant bending response and the stable mechanical properties of hydrogel actuators is very important and greatly challenging.

In this work, we present a simple and reliable strategy to prepare a temperature-responsive, gradient porous hydrogel by controlling the deposition of montmorillonite (MMT) in the copolymerization of the *N*-isopropylacrylamide (NIPAM) monomer. Compared with the pure poly(*N*-isopropylacrylamide) (PNIPAM) hydrogel without MMT, the as-obtained composite hydrogel with MMT possessed a lower volume phase transition temperature (VPTT) and a faster water loss rate in water at 50 °C, which led to faster deformation of the hydrogel. Also, the bending direction and the bending rate of the hydrogel could be regulated by controlling the content of MMT and the thickness of the hydrogel. These results suggest an effective route for intelligent hydrogel preparation and its potential application as a soft actuator in the future.

2. Materials and methods

2.1 Reagents and materials

NIPAM (98.0%), MMT K-10 ($Al_2O_9Si_3$), potassium persulphate (KPS) and *N*,*N*′-methylenebisacrylamide (MBAA) were purchased from Shanghai Macklin Biochemical Co., Ltd (China), and *N*,*N*,*N*′,*N*′-tetramethylethylenediamine (TEMED) was purchased from Shanghai Aladdin Chemical Agent Co., Ltd (China). The MMT K-10 was first treated in dilute H_2SO_4, centrifugally washed to neutral (pH = 7), dried at 60 °C overnight and finally ground into a powder for use. Deionized water (18.2 MΩ at 25 °C) from a water purification system (UPT-I-10, China) was used throughout the experiments. All reagents were of analytical grade.

2.2 Preparation of the gradient composite hydrogel

The MMT was ultrasonically dispersed in 10 mL deionized water, then 2.03 g of NIPAM and 0.002 g of MBAA were added to the solution under stirring for 30 min, and the mixture was degassed in a continuous nitrogen-saturated atmosphere for 5–10 min. Then 1.2 mL of the TEMED solution (7.75 mg mL^{-1}) and 1.5 mL of the KPS solution (10 mg mL^{-1}) were added into the above solution, and the mixture was injected into the mold (50 mm × 10 mm × 1 mm) composed of glass slides and silicone (Fig. 1a) and maintained horizontally for 24 hours in a closed space until an anisotropic composite hydrogel was obtained after NIPAM copolymerization to form PNIPAM.

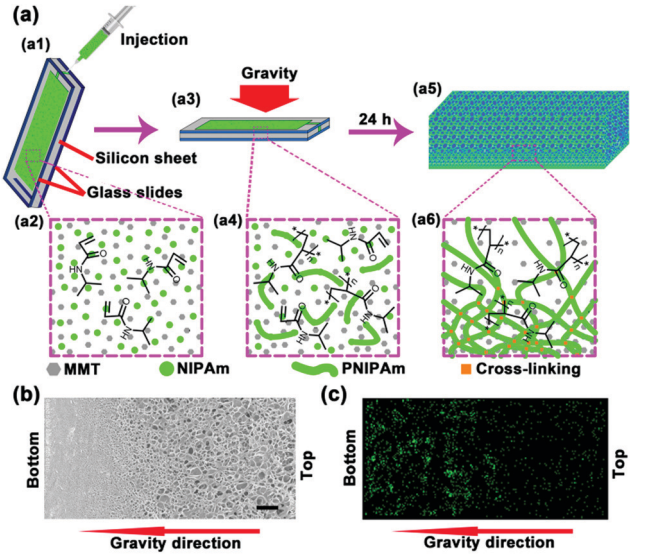

Fig. 1 (a) Schematic synthesis of the anisotropic gradient composite hydrogel (a1–a4), polymerization dispersion (a5), and gradient network structure (a6). (b) SEM image and (c) the corresponding mapping of the Si element in the cross section of the freeze-dried 0.2 MN composite hydrogel with a large-ranging gradient structure along the direction of gravity. The scale bars of (b) and (c) are 10 μm.

Since the precursor of the composite hydrogel contained MMT and NIPAM, and the amount of MMT was changed from 0.05 g to 0.3 g, the anisotropic composite hydrogel was therefore labeled as '*x*MN' (*x* is the mass concentration ratio of MMT to deionized water in the precursor dispersion, the values of which were 0.05, 0.3 and so on). A pure PNIPAM hydrogel without MMT was also prepared as a contrast according to the similar process described above.

In order to realize flexible and complicated deformation, patterned hydrogels were prepared by injecting the precursor into a well-designed mold with different local thicknesses. In order to explore the light induced temperature responsive performance, carbon nanotubes (Beijing DK Daojin Nano technology Co. Ltd, China) were mixed with MMT at a mass ratio of 1 : 10 in an agate mortar for 10 minutes, and the resulting products (MMT/CNTs) with light-to-heat conversion performance were used to prepare light responsive composite hydrogels.

2.3 Characterization of the composite hydrogel

The morphology and microstructure of the hydrogels were observed by scanning electron microscopy (SEM, S-4800, Hitachi) at the accelerated voltage of 5 kV. Before the measurement, the samples were frozen in liquid nitrogen and then freeze-dried in a cold trap (FD-1A-80, China) at −90 °C. The relative thickness of the bottom layer of the MMT deposition was observed by inverted fluorescence microscopy (Carl Zeiss Microscopy GmbH, 37081 Gottingen, Germany). Fourier transform infrared (FT-IR) spectroscopy measurements were carried out on a Nicolet 6700 spectrometer using KBr disks in the scanning range from 450 cm^{-1} to 4000 cm^{-1}.

The VPTT of the composite hydrogel was analyzed on a differential scanning calorimeter (DSC, TA DSC Q200, USA) by

heating the sample from 20 °C to 50 °C at a scanning rate of 5 °C min^{-1} under nitrogen. The swelling and deswelling kinetics were determined by measuring the temporal weight change of the hydrogels. For the swelling (or reswelling) kinetic study, the hydrogels with the deswelling equilibrium at 50 °C were first swelling-equilibrated in deionized water at a certain temperature (20 °C) and were weighed at a given time. The equilibrium reswelling ratio (RR) was calculated as follows:

$$\mathrm{RR} = \frac{W_t - W_\mathrm{d}}{W_\mathrm{d}} \times 100\%, \quad (1)$$

where W_t is the weight of the swollen hydrogel at a given time during swelling (or reswelling) and W_d is the weight of the dry hydrogel. For the deswelling kinetic study, the fully swelled hydrogel at 20 °C was rapidly transferred into 50 °C hot water. The water retention ratio (WR) was defined as the percentage of water content at a certain time relative to the initial equilibrium water content, namely

$$\mathrm{WR} = \frac{W_t' - W_\mathrm{d}}{W_\mathrm{s} - W_\mathrm{d}} \times 100\%, \quad (2)$$

where W_t' is the weight of the hydrogel at a given time interval during the course of deswelling and W_s is the weight of the equilibrium swollen hydrogel at 20 °C. The compressive mechanical properties of the composite hydrogel were evaluated by using the mechanical testing machine (INSTRON 5943, USA). The size of the samples for the stress–strain curve measurement was 20 mm in diameter and 16 mm in height.

In order to investigate the bending behavior of composite hydrogels, one end of the hydrogel was fixed with a clip, while the other end was free to suspend in the air. Then, the hydrogel was immersed in deionized water at 50 °C to record the time and bending angle. The difference between the maximum bending angle and the initial bending angle was defined as the amplitude. The laser stimulated temperature-responsive behavior of the gradient composite hydrogel was studied *via* the near-infrared (NIR) illumination system by using a NIR laser with a wavelength of 808 nm (Model LSR808H-10W, Ningbo Yuanming Laser Technology Co., Ltd, China). The distance between the laser source and the sample was 20 cm. The power of the NIR laser was 2.0 W.

3. Results and discussion

3.1 Preparation and microstructure of the composite hydrogel

The fabrication process of the porous composite hydrogel is schematically illustrated in Fig. 1a1–a6. As shown, the formation of the anisotropic structure of the hydrogel is mainly due to the MMT precipitation under gravity (Fig. 1a3) and the NIPAM monomer copolymerization. Briefly, the precursor evenly dispersing the NIPAM monomer and MMT was injected into a mold (Fig. 1a1 and a2). As the polymerization process proceeded, the viscosity of the precursor became larger and larger, resulting in slower and slower precipitation of MMT (Fig. 1a4), so that the composite hydrogel had a component gradient of MMT in the direction of gravity. At the same time, the NIPAM monomer was easily adsorbed to the rough MMT surface (Fig. S1a, ESI†), resulting in a cross-linking gradient of the MMT component along the direction of the gradient during polymerization (Fig. 1a5 and a6). The gradient network structure (Fig. 1b) and gradient composition distribution (Fig. 1c) in the 0.2 MN composite hydrogel, for example, is demonstrated *via* SEM observation along the direction of gravity. The elemental mapping analysis (Fig. 1c) showed a higher content of Si (MMT) at the bottom layer than at the top one. Compared with the uniform porous structure in the pure PNIPAM hydrogel (Fig. S1b, ESI†), the composite hydrogel possessed a gradient porous structure with smaller pores in the bottom layer (Fig. S1c, ESI†) and larger ones in the top layer (Fig. S1d, ESI†). This special gradient structure indicates that the temperature-responsive composite hydrogel will have different degrees of shrinking and deformation under external thermal stimulus. The MMT incorporation in the hydrogel network was also confirmed *via* FT-IR spectroscopy measurements (Fig. S2, ESI†). The characteristic peaks at 1542 cm^{-1}, 1654 cm^{-1} and 3288 cm^{-1} are assigned to the amides II, carbonyl group (C═O) and N–H bonds from PNIPAM, respectively. The characteristic peaks related to the Si–O and Mg–O groups in MMT are located at about 500 cm^{-1} and 1000 cm^{-1}, respectively.[42,43]

3.2 Phase transition and swelling/deswelling kinetics of the composite hydrogel

It is well known that the temperature-sensitive PNIPAM hydrogel is in a swollen state in water due to the hydrogen bonds formed between water molecules and the N–H or C═O groups of NIPAM below the lower critical solution temperature (LCST). However, it displays abrupt volume shrinkage due to the dehydration of hydrophobic isopropyl groups and hydrophilic amide groups when the environmental temperature is higher than the LCST. Since the hydrophobic isopropyl groups have a smaller time constant of 109 ± 64 ns than that of hydrophilic amide groups (360 ± 85 ns) during the dehydration process, they initiate the volume collapse of PNIPAM.[44,45] Therefore, two distinct endothermic peaks at about 31 °C and 32 °C in the DSC curves of PNIPAM (Fig. 2a) may be due to the dehydration of isopropyl groups and amide groups, respectively.[46] When hydrophobic MMT was added into PNIPAM, more water molecules might aggregate around the hydrophobe, indicating the occurrence of the VPTT at a lower temperature.[47,48] A similar result was also found in hydrophobic component-containing PNIPAM hydrogels.[47] However, the amount of MMT in the composite hydrogels does not affect the VPTT obviously. Therefore, the top and bottom sides with different MMT contents present almost the same VPTT (Fig. 2a). Since MMT does not undergo any phase transition at around 30 °C, the *x*MN samples containing MMT present a lower heat flow when considering the unit mass, and the heat flow rates of pure PNIPAM, *x*MN-top and *x*MN-bottom are 4.10 W g^{-1}, 1.43 W g^{-1} and 1.09 W g^{-1}, respectively.

The MMT incorporation also affected the swelling (or reswelling) kinetics of the hydrogels. As shown in Fig. 2b, the RR for composite hydrogels gradually decreases with the increasing MMT content.

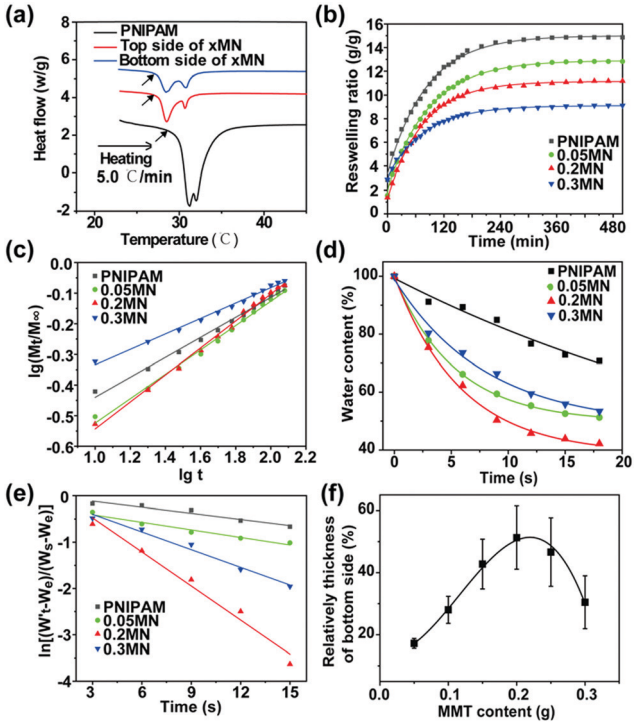

Fig. 2 (a) DSC curves of pure PNIPAM without MMT and the two sides of the *x*MN composite hydrogel. (b) Reswelling kinetic curves of the composite hydrogels at 20 °C. (c) Plots of $\lg(M_t/M_\infty)$ against $\lg t$ for the composite hydrogels. (d) Deswelling behavior of the composite hydrogels at 50 °C. (e) $\ln[(W_t' - W_e)/(W_s - W_e)]$ *versus* time t for the composite hydrogels at 50 °C. (f) Relative thickness of the bottom side of the composite hydrogels with different MMT contents.

When a small amount of MMT (such as 0.05 g) is added into the hydrogel network, it disperses well in the nanocomposite hydrogel as a crosslinker, and the pore structure is almost uniform similar to that of the pure PNIPAM hydrogel except a few small holes on the bottom part (Fig. S3a, ESI†). With the further increase of the MMT content in the composite hydrogels (from 0.1 g to 0.2 g), superabundant MMT would deposit at the bottom of the hydrogels under gravity, and much denser networks form at the bottom of the hydrogel, blocking the flowing channels of free water. When the MMT content increases to 0.3 g, the bottom layer is almost compacted with the RR decrease by half. In order to investigate the water uptake process of hydrogels, the initial reswelling data were treated and fitted with the exponential heuristic equation

$$\frac{M_t}{M_\infty} = Kt^n, \tag{3}$$

where M_t and M_∞ are the amounts of water uptake at time t and after reswelling for 500 min, respectively; K is the characteristic constant of the hydrogel; and n is a characteristic exponent related to the transport mode. Our results indicate that the n value is near 0.5, which indicates that the transport process of water penetrating into the hydrogel is controlled by Fickian diffusion.[49,50]

The deswelling behavior of the equilibrium-swollen composite hydrogels was studied in water at 50 °C. It can be seen that the pure PNIPAM hydrogel presents a relatively slow water loss when immersed in water at 50 °C and its rate remains at a constant value between 0 and 18 s (Fig. 2d). The 0.2 MN composite hydrogel exhibits a much higher response rate, which might be attributed to the quick water loss through many small holes combined with the lower water content in this hydrogel. As observed by SEM, a thicker and denser porous bottom layer is formed for the 0.2 MN composite hydrogels (Fig. S3d and S4d, ESI†) owing to the presence of a large amount of MMT in the hydrogel system. When the MMT content in the composite hydrogel increases to 0.3 g, the water loss rate of the 0.3 MN composite hydrogel decreases unexpectedly (Fig. 2d). According to the optical microscopic images (Fig. S4, ESI†) and Si element mapping (Fig. S5, ESI†) for the cross section of composite hydrogels with different MMT contents, the thickness ratio of the bottom layer to the total hydrogel layer shows a tendency to increase first and decrease later (Fig. 2f), indicating that too much MMT at the bottom layer of the 0.3 MN composite hydrogel could supply fewer water-releasing channels and therefore present slower dehydration. The stress–strain tests (Fig. S6, ESI†) for the pure PNIPAM hydrogel and composite hydrogels with different MMT contents were performed under the same conditions. Compared with the other three samples, the elastic modulus of the 0.3 MN composite hydrogel is enhanced significantly, revealing that excess MMT particles induce a denser network in the composite hydrogel. In addition, the deswelling process of hydrogels was quantitatively analyzed by using the following equation

$$\ln[(W_t' - W_e)/(W_s - W_e)] = -kt, \tag{4}$$

where W_e is the weight of hydrogels in the equilibrium deswelling state, t is the deswelling time, and k is the deswelling rate. The plots of $\ln[(W_t' - W_e)/(W_s - W_e)]$ against time t for all hydrogels are linear (Fig. 2e) with the deswelling rate constants k of 0.04 (PNIPAM), 0.05 (0.05 MN), 0.25 (0.2 MN) and 0.13 (0.3 MN), respectively, indicating that the deswelling process can be approximately governed in a first-ordered manner.[49,51] The higher deswelling rate for the 0.2 MN composite hydrogel is due to the increased crosslinking densities and structure with more small holes.

3.3 Temperature-responsive driving behavior of the composite hydrogel

The driving performance of the hydrogel under temperature stimulus was evaluated by measuring the bending angle (θ) in water at 50 °C (Fig. 3a). Here θ_1 and θ_2 are the angles between the longitudinal axis and the tangent line at the end of the hydrogel strip when the strip bends towards the left and right sides, respectively. When the hydrogel strip is curled with the θ value over 180° and 360° (Fig. S7, ESI†), the computational formula for θ is given in the ESI.† It should be noticed that the isotropous pure PNIPAM hydrogel displays only volume shrinkage without bending behavior in water at 50 °C (Fig. S8a, ESI†). Nevertheless, the temperature-responsive bending characteristics of the composite hydrogel were realized by the design of the asymmetric gradient structure of the composite

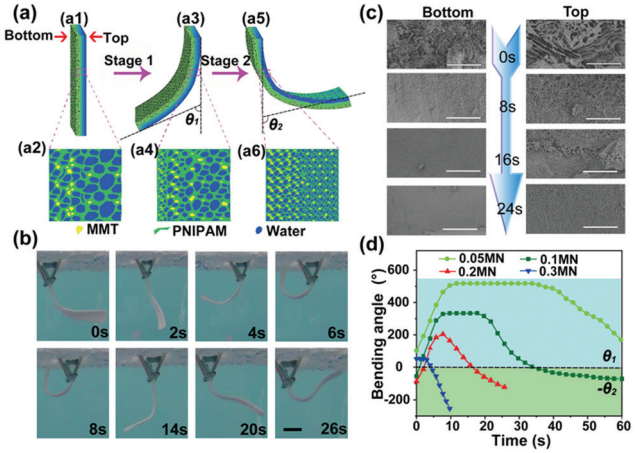

Fig. 3 (a) Schematic illustration of the temperature-responsive bending mechanism of the composite hydrogel. θ_1 and θ_2 are the bending angles of the two stages. (a1), (a3) and (a5) are the bent positions in different stages; and (a2), (a4) and (a6) are the corresponding schematic networks. (b) Optical photographs of the bending process of the 0.2 MN composite hydrogel with a thickness of 1 mm in water at 50 °C. The scale bar is 10 mm. (c) SEM images of the cross sections of the 0.2 MN composite hydrogel at the top and bottom sides at different stages in water at 50 °C. The scale bar is 100 μm. (d) The relationship between the bending angle and the time of different hydrogels in water at 50 °C.

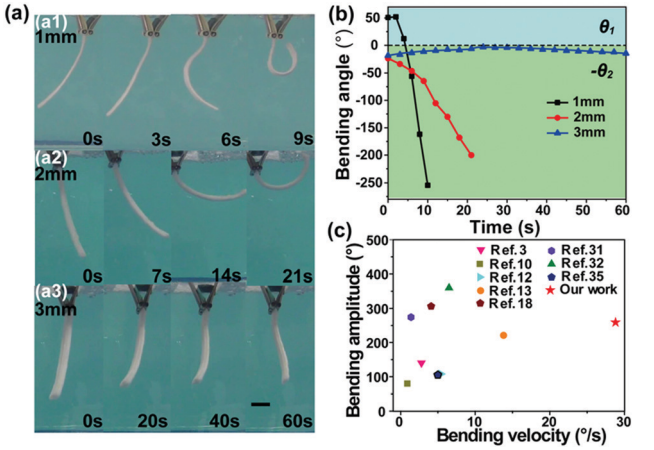

Fig. 4 (a) Bending deformation of the 0.3 MN composite hydrogels with different thicknesses in water at 50 °C. The scale bar is 10 mm. (b) The relationship between the bending angle and time for the 0.3 MN composite hydrogels with different thicknesses in water at 50 °C. (c) Comparison of the bending velocity and bending amplitude of different hydrogel actuators. Detailed information is given in Table S1 (ESI†).

hydrogel *via* MMT precipitation under gravity. For the 0.2 MN composite hydrogel with a thickness of 1 mm, as schematically shown in Fig. 3a1, when the surrounding temperature is lower than the VPTT of PNIPAM, the composite hydrogel is naturally suspended. However, when the composite hydrogel is immersed in water at 50 °C, the bottom side with MMT enrichment shrinks faster and generates a larger resultant force than the top side,[31] which leads to the bending of the hydrogel strip toward the bottom side between 0 and 8 s (Fig. 3a3, b and d). At the 8th second, the bottom side of the 0.2 MN composite hydrogel almost reaches maximum contraction, but there is still a lot of shrinkable space on the top side (Fig. 3a4 and c). Therefore, the top side of the composite hydrogel continues to shrink, resulting in a reversed bending of the hydrogel strip (Fig. 3a5, b, d and Movie S1, ESI†). When the MMT content in the composite hydrogel is below 0.2 g, the hydrogel becomes softer with the decrease of the MMT content, leading to a larger bending angle toward the bottom side. Meanwhile, the bending angle of the hydrogel is stuck for some time due to the great degree of shrinkage and the bonding between polymers (Fig. 3d and Fig. S8b, c, ESI†).[31,33] More interestingly, when the MMT content arrives at 0.3 g, the composite hydrogel only presents bending towards the top side (Fig. 3d and Fig. S8d, ESI†), which could be ascribed to the very dense distribution of MMT at the bottom side of the 0.3 MN composite hydrogel with negligible space to shrink in the bottom side. The reversible bending response of the 0.2 MN and 0.3 MN composite hydrogels at 25 and 50 °C (the starting points are unified to 0°) is shown in Fig. S9 (ESI†). And the average bending speeds of the 0.2 MN and 0.3 MN composite hydrogel strips in the deswelling stage are 36.2, 33.3, 35.9, 31.9, 33.8° s^{-1} and −30.5, −27.9, −28.8, −27.9, −26.8° s^{-1}, respectively, with the standard deviations of 1.80 and 1.40, indicating their excellent stability and reproducibility. After repeated deswelling–reswelling tests, the 0.3 MN composite hydrogel strip was placed in water at room temperature for one week to retest. The response reduces about 20% after one-month measurement due to the degradation of performance (Fig. S10, ESI†).

In addition, the thickness of the hydrogel also greatly affects the actuation behavior of the composite hydrogel.[52] The bending behaviors of the 0.3 MN composite hydrogels with different thicknesses in water at 50 °C are shown in Fig. 4a and b. It can be seen that the composite hydrogel with a thickness of 1 mm can be bent −259° within 9 s (Movie S2, ESI†), and the bending speed is estimated to be about −28.8° s^{-1}, which is much larger than those of the composite hydrogel with a thickness of 2 mm (−177° within 21 s at a speed of −8.4° s^{-1}) (Movie S3, ESI†) and the composite hydrogel with a thickness of 3 mm (which is almost unbent within 60 s, Movie S4, ESI†). Also, our optimized temperature-responsive hydrogel actuator has a fast bending velocity with a large bending amplitude when compared to many hydrogel actuators (Fig. 4c). Therefore, artificial design for the local thickness of a composite hydrogel can effectively adjust its bending behavior.

3.4 Flexibly controllable deformation of the composite hydrogel as a soft actuator

Through the enlightenment of the effects of the MMT content and hydrogel thickness on the bending behavior, we design a patterned gradient composite hydrogel as a soft actuator to realize some special deformation. For example, a four-arm gripper with a thickness of 1 mm was manufactured through a cross-shaped die (Fig. 5a1). This hydrogel manipulator (the top side is down) of the 0.3 MN hydrogel sheet with its center connected to a wire can be used as a claw to pick up targeted objects in the water bath at 50 °C and transfer and release it to

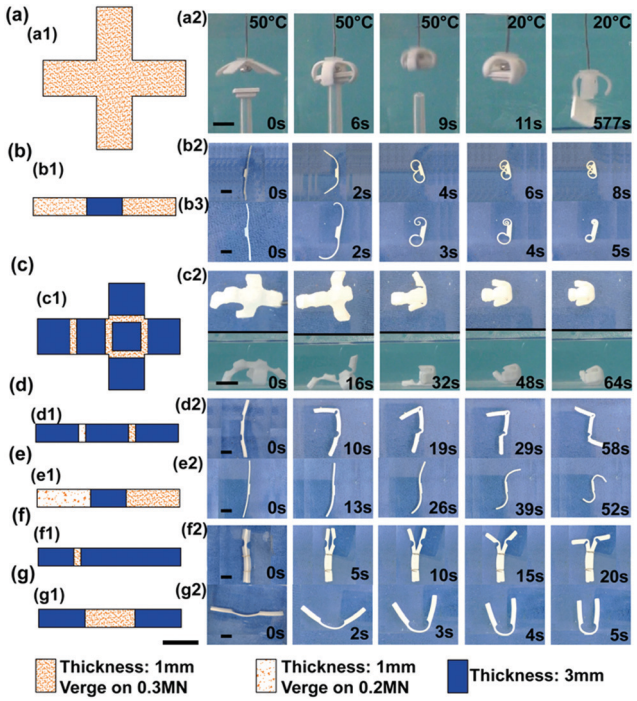

Fig. 5 (a1–g1) Schematic illustration of the design of hydrogel actuators. (a2) Capture and transportation of a cuvette lid by a moving cross-shaped 0.3 MN hydrogel actuator as the gripper. (b2) Symmetrical deformation of the 0.3 MN composite hydrogels with a local thickness difference in water at 50 °C. (b3) Asymmetric deformation of the 0.3 MN composite hydrogels with local thickness difference and MMT content difference in water at 50 °C. (c2) Closure of the box type hydrogel actuator in water at 50 °C. (d2–g2) Hydrogel actuators with different local thicknesses and MMT contents form the shapes of the capital letters "Z", "S", "T" and "U" ("ZSTU" is the abbreviation of Zhejiang Sci-Tech University) in water at 50 °C. All the scale bars are 10 mm.

another vessel with water at 20 °C (Fig. 5a2 and Movie S5, ESI†) by rapidly bending toward the top side at 50 °C and subsequently unfolding at 20 °C. Moreover, well-designed molds with different local thicknesses were used to construct the patterned hydrogel by adjusting the bending position, bending direction and bending amplitude in order to realize the complexly controllable motion of soft actuators. First, we design a triarticular soft stripe (0.3 MN composite hydrogel) with the thickness of the middle part (3 mm) being larger than those of both ends (1 mm). If these two ends have a symmetrical distribution of MMT in the 0.3 MN composite hydrogel, the soft stripe presents a symmetric crimp towards the middle part in the horizontal plane in water at 50 °C (Fig. 5b2 and Movie S6, ESI†); otherwise, both ends present an asymmetrical curl towards the center line (Fig. 5b3 and Movie S7, ESI†) due to the asynchronous deformation of the hydrogel with asymmetric MMT distribution in it (the mold was placed on a bevel during the composite hydrogel polymerization). The soft hydrogel actuator can also achieve a sophisticated 3D folding movement. Given that the actuator has only a very short section to bend and the other parts are not responsive, the actuator would change from slow bending to sharp bending, thus presenting a folding mechanism.[53] Based on this simple concept, a cardboard box actuator was designed with the link parts thinner than carton surfaces (Fig. 5c1). When immersed in hot water at 50 °C, the cardboard could fold automatically along the direction we expected and form a closed box at about 60 s (Fig. 5c2 and Movie S8, ESI†). Similarly, the letter actuators were also constructed to realize the deformation of "Z", "S", "T" and "U" (the abbreviation of Zhejiang Sci-Tec University) in water at 50 °C (Fig. 5d–g and Movie S9–S12, ESI†). In order to realize the bending of two ends of soft actuators towards completely opposite directions (such as "Z" and "S"), the MMT contents for two joints are controlled to be 0.2 MN and 0.3 MN, respectively. Therefore, the controlled deformation of temperature-responsive soft actuators can be intentionally designed by adjusting the shape, local MMT content and thickness of the composite hydrogel with heterogeneous structures.

In addition, the temperature-responsive performance of the PNIPAM-based composite hydrogel induced by the photothermal stimulus is realized by mixing CNTs with MMT. Because light-responsive CNTs are distributed with MMT in the bottom side of the actuator rather than in the whole 0.3 MN composite hydrogel due to the hydrophobicity of CNTs,[54] the top side of the hydrogel can produce greater swelling in water at 20 °C, which causes the actuator to bend toward the bottom side (Fig. S11a, ESI†). When a point laser source was used to stimulate the actuator in water at 20 °C, it can continue to bend toward the bottom side due to the heated CNTs with photo-thermal sensitivity, resulting in shrinkage of the bottom side (Fig. S11b, ESI†).

4. Conclusions

In summary, we have reported here a temperature-responsive actuator using an anisotropic gradient PNIPAM-based hydrogel *via* a simple and reliable method. The anisotropic composite hydrogel showed distinguished performances such as rapid actuation in water at 50 °C, adjustable bending direction, bending angle and bendable position. Among them, the representative composite hydrogels were 0.2 MN hydrogel with bidirectional bending characteristics and 0.3 MN hydrogel with unidirectional bending ability. The bending amplitude of the 0.2 MN composite hydrogel in the first stage was about 289° and the average bending speed was about 36° s^{-1}. Furthermore, the 0.3 MN composite hydrogel also displayed a fast bending velocity ($\sim -28.8°\ s^{-1}$) with a large bending amplitude ($\sim -259°$). Also, the flexibly controllable deformation of the hydrogel actuator was specified by designing patterned hydrogels with different local thicknesses and components. This simple and reliable solution could be used in the future design and manufacture of hydrogel-based driving materials which have potential applications in the fields of soft robots and smart drivers.

Conflicts of interest

There are no conflicts to declare.

Acknowledgements

This work was supported by the Zhejiang Outstanding Youth Fund (No. LR19E020004), the National Natural Science Foundation of China (No. 11672269 and 11972323), the Zhejiang Provincial Natural Science Foundation of China (No. LR20A020002), the Opening Fund of the State Key Laboratory for Strength and Vibration of Mechanical Structures (Xi'an Jiaotong University) (No. SV2018-KF-23), the China Scholarship Council (No. 201908330181), and the Fundamental Research Funds for the Provincial Universities of Zhejiang (No. RF-B2019004).

Notes and references

1 S. R. Shin, B. Migliori, B. Miccoli, Y. C. Li, P. Mostafalu, J. Seo, S. Mandla, A. Enrico, S. Antona and R. Sabarish, *Adv. Mater.*, 2018, **30**, 1704189.
2 P. Calvert, *Adv. Mater.*, 2009, **21**, 743–756.
3 W. J. Zheng, N. An, J. H. Yang, J. Zhou and Y. M. Chen, *ACS Appl. Mater. Interfaces*, 2015, **7**, 1758–1764.
4 N. Tao, D. Zhang, X. Li, D. Lou, X. Sun, C. Wei, J. Li, J. Yang and Y.-N. Liu, *Chem. Sci.*, 2019, **10**, 10765–10771.
5 J. Deng, W. Liang and J. Fang, *ACS Appl. Mater. Interfaces*, 2016, **8**, 3928–3932.
6 M. A. Stuart, W. T. Huck, J. Genzer, M. Muller, C. Ober, M. Stamm, G. B. Sukhorukov, I. Szleifer, V. V. Tsukruk, M. Urban, F. Winnik, S. Zauscher, I. Luzinov and S. Minko, *Nat. Mater.*, 2010, **9**, 101–113.
7 D. Zhang, Y. Fu, L. Huang, Y. Zhang, B. Ren, M. Zhong, J. Yang and J. Zheng, *J. Mater. Chem. B*, 2018, **6**, 950–960.
8 H.-Y. Peng, W. Wang, F. Gao, S. Lin, L.-Y. Liu, X.-Q. Pu, Z. Liu, X.-J. Ju, R. Xie and L.-Y. Chu, *J. Mater. Chem. C*, 2018, **6**, 11356–11367.
9 Y. Tan, D. Wang, H. Xu, Y. Yang, W. An, L. Yu, Z. Xiao and S. Xu, *Macromol. Rapid Commun.*, 2018, **39**, 1700863.
10 E. Zhang, T. Wang, W. Hong, W. Sun, X. Liu and Z. Tong, *J. Mater. Chem. A*, 2014, **2**, 15633–15639.
11 Z. Hu, X. Zhang and Y. Li, *Science*, 1995, **269**, 525–527.
12 Q. Zhao, Y. Liang, L. Ren, Z. Yu, Z. Zhang, F. Qiu and L. Ren, *J. Mater. Chem. B*, 2018, **6**, 1260–1271.
13 X. He, Y. Sun, J. Wu, Y. Wang, F. Chen, P. Fan, M. Zhong, S. Xiao, D. Zhang, J. Yang and J. Zheng, *J. Mater. Chem. C*, 2019, **7**, 4970–4980.
14 L. Yang, K. Qi, L. Chang, A. Xu, Y. Hu, H. Zhai and P. Lu, *J. Mater. Chem. B*, 2018, **6**, 5031–5038.
15 M. R. Islam, X. Li, K. Smyth and M. J. Serpe, *Angew. Chem., Int. Ed.*, 2013, **52**, 10330–10333.
16 M. Dai, O. T. Picot, J. M. N. Verjans, L. T. de Haan, A. P. H. J. Schenning, T. Peijs and C. W. M. Bastiaansen, *ACS Appl. Mater. Interfaces*, 2013, **5**, 4945–4950.
17 C. Ma, T. Li, Q. Zhao, X. Yang, J. Wu, Y. Luo and T. Xie, *Adv. Mater.*, 2014, **26**, 5665–5669.
18 L. Zhao, J. Huang, Y. Zhang, T. Wang, W. Sun and Z. Tong, *ACS Appl. Mater. Interfaces*, 2017, **9**, 11866–11873.
19 Y. Cheng, C. Huang, D. Yang, K. Ren and J. Wei, *J. Mater. Chem. B*, 2018, **6**, 8170–8179.
20 S. J. Kim, H. I. Kim, S. J. Park, I. Y. Kim, S. H. Lee, T. S. Lee and S. I. Kim, *Smart Mater. Struct.*, 2005, **14**, 511–514.
21 Y. Osada, H. Okuzaki and H. Hori, *Nature*, 1992, **355**, 242–244.
22 B. Xue, M. Qin, T. Wang, J. Wu, D. Luo, Q. Jiang, Y. Li, Y. Cao and W. Wang, *Adv. Funct. Mater.*, 2016, **26**, 9053–9062.
23 Q. Li, X. Wang, L. Dong, C. Liu and S. Fan, *Soft Matter*, 2019, **15**, 9788–9796.
24 R. Fuhrer, E. K. Athanassiou, N. A. Luechinger and W. J. Stark, *Small*, 2009, **5**, 383–388.
25 F. Gao, N. Zhang, X. Fang and M. Ma, *J. Mater. Chem. C*, 2017, **5**, 4129–4133.
26 R. Cheng, L. Zhu, W. Huang, L. Mao and Y. Zhao, *Soft Matter*, 2016, **12**, 8440–8447.
27 M. Kondo, Y. Yu and T. Ikeda, *Angew. Chem., Int. Ed.*, 2006, **45**, 1378–1382.
28 H. Thérien-Aubin, Z. L. Wu, Z. Nie and E. Kumacheva, *J. Am. Chem. Soc.*, 2013, **135**, 4834–4839.
29 L. Wang, Y. Jian, X. Le, W. Lu, C. Ma, J. Zhang, Y. Huang, C.-F. Huang and T. Chen, *Chem. Commun.*, 2018, **54**, 1229–1232.
30 X. Li, X. Cai, Y. Gao and M. J. Serpe, *J. Mater. Chem. B*, 2017, **5**, 2804–2812.
31 C. Yao, Z. Liu, C. Yang, W. Wang, X.-J. Ju, R. Xie and L.-Y. Chu, *Adv. Funct. Mater.*, 2015, **25**, 2980–2991.
32 J. Zheng, P. Xiao, X. Le, W. Lu, P. Théato, C. Ma, B. Du, J. Zhang, Y. Huang and T. Chen, *J. Mater. Chem. C*, 2018, **6**, 1320–1327.
33 J. Wang, J. Wang, Z. Chen, S. Fang, Y. Zhu, R. H. Baughman and L. Jiang, *Chem. Mater.*, 2017, **29**, 9793–9801.
34 Y. Tan, R. Wu, H. Li, W. Ren, J. Du, S. Xu and J. Wang, *J. Mater. Chem. B*, 2015, **3**, 4426–4430.
35 Y. Tan, D. Wang, H. Xu, Y. Yang, X. L. Wang, F. Tian, P. Xu, W. An, X. Zhao and S. Xu, *ACS Appl. Mater. Interfaces*, 2018, **10**, 40125–40131.
36 K. Haraguchi and H.-J. Li, *Angew. Chem., Int. Ed.*, 2005, **44**, 6500–6504.
37 W. Fan, C. Shan, H. Guo, J. Sang, R. Wang, R. Zheng, K. Sui and Z. J. S. A. Nie, *Sci. Adv.*, 2019, **5**, eaav7174.
38 X. Zhang, C. L. Pint, M. H. Lee, B. E. Schubert, A. Jamshidi, K. Takei, H. Ko, A. Gillies, R. Bardhan, J. J. Urban, M. Wu, R. Fearing and A. Javey, *Nano Lett.*, 2011, **11**, 3239–3244.
39 R. M. Erb, J. S. Sander, R. Grisch and A. R. Studart, *Nat. Commun.*, 2013, **4**, 1712–1719.
40 S. Y. Zheng, Y. Tian, X. N. Zhang, M. Du, Y. Song, Z. L. Wu and Q. Zheng, *Soft Matter*, 2018, **14**, 5888–5897.
41 R. Luo, J. Wu, N.-D. Dinh and C.-H. Chen, *Adv. Funct. Mater.*, 2015, **25**, 7272–7279.
42 S. Bucatariu, G. Fundueanu, I. Prisacaru, M. Balan, I. Stoica, V. Harabagiu and M. Constantin, *J. Polym. Res.*, 2014, **21**, 580–591.
43 M. R. Kaiser, H. Anuar and S. B. A. Razak, *J. Thermoplast. Compos. Mater.*, 2012, **27**, 992–1009.
44 B. Ziółkowski, L. Florea, J. Theobald, F. Benito-Lopez and D. Diamond, *J. Mater. Sci.*, 2015, **51**, 1392–1399.
45 C. Boutris, E. Chatzi and C. Kiparissides, *Polymer*, 1997, **38**, 2567–2570.

46 S. Shekhar, M. Mukherjee and A. K. Sen, *Adv. Mater. Res.*, 2012, **1**, 269–284.
47 J. Gan, X. Guan, J. Zheng, H. Guo, K. Wu, L. Liang and M. Lu, *RSC Adv.*, 2016, **6**, 32967–32978.
48 H. I. Kim and K. Ishihara, *Biomat. Biomed. Eng.*, 2014, **1**, 95–104.
49 J. Ma, L. Zhang, B. Fan, Y. Xu and B. Liang, *J. Polym. Sci. Pol. Phys.*, 2008, **46**, 1546–1555.
50 X. Jin and Y.-L. Hsieh, *Polymer*, 2005, **46**, 5149–5160.
51 T. Serizawa, K. Wakita and M. Akashi, *Macromolecules*, 2002, **35**, 10–12.
52 Y. Li and T. Tanaka, *J. Chem. Phys.*, 1990, **92**, 1365–1371.
53 K.-U. Jeong, J.-H. Jang, D.-Y. Kim, C. Nah, J. H. Lee, M.-H. Lee, H.-J. Sun, C.-L. Wang, S. Z. D. Cheng and E. L. Thomas, *J. Mater. Chem.*, 2011, **21**, 6824–6830.
54 J. Pu, S. Wan, Z. Lu, G.-A. Zhang, L. Wang, X. Zhang and Q. Xue, *J. Mater. Chem. A*, 2013, **1**, 1254–1260.